ARTICLE

Check for updates

Stacking and spin order in a van der Waals Mott insulator 1T-TaS$_2$

Jae Whan Park [1✉], Jinwon Lee [1,2,3] & Han Woong Yeom [1,2✉]

Quasi-two-dimensional charge density wave system of 1T-TaS$_2$ has attracted recent interest due to topological excitations, emergent superconductivity, ultrafast synaptic functionality, and the possibility of a quantum spin liquid state. While electron correlation has been known to be essential in this system, the nature of its insulating phase is currently under debate. Here, we reinvestigate the origin of the insulating band structures of the 1T-TaS$_2$ surface using density-functional theory calculations to consider the recently-raised issues such as interlayer coupling, surface effect, and interlayer spin ordering. We identify four distinct electronic states of the surface layer such as a 2D Mott phase, a strongly-coupled anti-ferromagnetic insulator, a weakly-coupled ferromagnetic insulator, and a small-gap semi-conductor, depending on types of the surface termination and the interlayer spin configuration. These distinct surface electronic states explain the different sizes of spectro-scopic band gaps observed in scanning tunneling microscopy, revealing the complexity of the interlayer charge and spin couplings in layered correlated materials.

[1] Center for Artificial Low Dimensional Electronic Systems, Institute for Basic Science (IBS), Pohang 37673, Republic of Korea. [2] Department of Physics, Pohang University of Science and Technology (POSTECH), Pohang 37673, Republic of Korea. [3] Present address: Department of Quantum Nanoscience, Kavli Institute of Nanoscience, Delft University of Technology, Delft 2628 CJ, The Netherlands. ✉email: absolute81@ibs.re.kr; yeom@postech.ac.kr

A layered transition metal dichalcogenides of 1T-TaS$_2$ has attracted significant research effort for its intriguing electronic properties and functionalities associated with its charge density wave (CDW) phase and, presumably, substantial effects of electron correlation. Topics discussed so far include the CDW mechanism, discommensurations in CDW, the realization of a 2D Mott insulating phase, emerging superconductivity under pressure and doping[1], ultrafast resistivity switchings[2], domain-wall topological excitations[3], and the possibility of an exotic quantum spin liquid state[4,5]. Except for the electron–phonon interaction to induce the CDW state, most of the above issues have been discussed under the light of substantial electron correlation of a partially filled band of well-localized Ta d electrons provided by the CDW structure, so-called, the David-star (DS) structure (Fig. 1a). For a few decades, this partially filled d band has been thought to fall into a Mott insulating state assuming a simplified 2D single-layer model[6,7].

However, the 2D Mott physics of the commensurate CDW phase in 1T-TaS$_2$ is under strong debate recently with renewed inputs from both experiments and theory, which revealed evidence of substantial interlayer interaction[8–10]. Bulk 1T-TaS$_2$ in its low-temperature ground state of a commensurate CDW phase is known to have an alternating bilayer structure called the AC stacking (see Fig. 1b), where two adjacent layers are stacked without a lateral transition (the A stacking) and each bilayer stacked with a ±2$\mathbf{a}$ translation (the C stacking) (Fig. 1b)[11]. Recent density-functional theory (DFT) studies suggested that half-filled $d_{z^2}^2$ orbitals at DS centers in each bilayer form a spin singlet state with a trivial bonding–antibonding gap in the A or AC stacking case[8,9]. The C stacking case was predicted to be metallic or to have a very small Mott gap with an interlayer antiferromagnetic (AFM) spin ordering[8,9,12]. A recent scanning tunneling spectroscopic (STS) study showed that surface layers after cleaving exhibit at least three distinct band gaps, a large gap of 0.4 eV for the A stacked surface (the type-I termination, see Fig. 1b), a small gap of 0.2 eV for a C stacked surface (type-II termination), and a metallic or partial gap in other types of stacking (faulted stackings)[10]. The Mott and bonding–antibonding nature of the small and large gaps were subsequently made clear by their distinct behaviors in the local charge doping by alkali adsorbates[13]. However, another very recent STS study showed a consistently large gap (0.4 eV) for all surface

terminations and suggested a stacking-independent Mott electronic state[14]. Moreover, the dichotomy of surface and bulk electronic states was also indicated by a recent ARPES study[15]. These updated experimental and theoretical results apparently do not converge into a single picture but suggest the complexity of this system and the existence of a hidden control parameter not considered so far.

In this study, we extensively investigate the possible electronic band structures of the 1T-TaS$_2$ surface layer with DFT calculations under different types of stackings, surface terminations, and interlayer spin couplings. We find that the 1T-TaS$_2$ surface can have four different types of band gap depending on stacking and spin couplings including an AFM bilayer of the A stacking, AFM and ferromagnetic (FM) couplings in the 2D-Mott single-layer of the C stacking, and a partial gap state in the B staking. Here, the Mott gap corresponds to the correlated band gap in the single-layer limit with minimal interlayer interaction, while the partial gap represents a correlated gap that is reduced by interlayer interaction. These four types of band gaps appear to explain consistently most of the previous observations by STS.

Results

Surface terminations and stacking orders

Among 13 Ta atomic sites in a CDW unit cell, five are symmetrically distinguishable[9], but we consider only three representative sites, A–C in Fig. 1a, for simplicity[14]. In the AC stacking order (the alternation of A and C stackings) assumed for the bulk, two different surface terminations are possible, type-I (interlayer) and type-II (intralayer) terminations shown in Fig. 1. The type-I(II) termination corresponds to an A(C)-stacked top layer as shown Fig. 1c(d). In recent transmission electron microscopy, stacking faults other than the AC stacking order were observed in a thin flake[16]. However, the thin flakes were differentiated from the bulk[16], and both electron microscopy and X-ray diffraction measurements confirmed a well-ordered AC stacking structure in bulk samples[11,15]. Nevertheless, we further considered the B stacking as a stacking fault and there can be B stacking cases in both type-I and type-II terminations as shown in the figure. Two other stacking fault structures (CC and AA stackings) are possible between the top and second layers as also shown in Fig. 1e and f, respectively. If one considers the interlayer coupling of DS spins, an interlayer AFM order becomes the ground state as suggested by the recent DFT studies for the bulk and surface
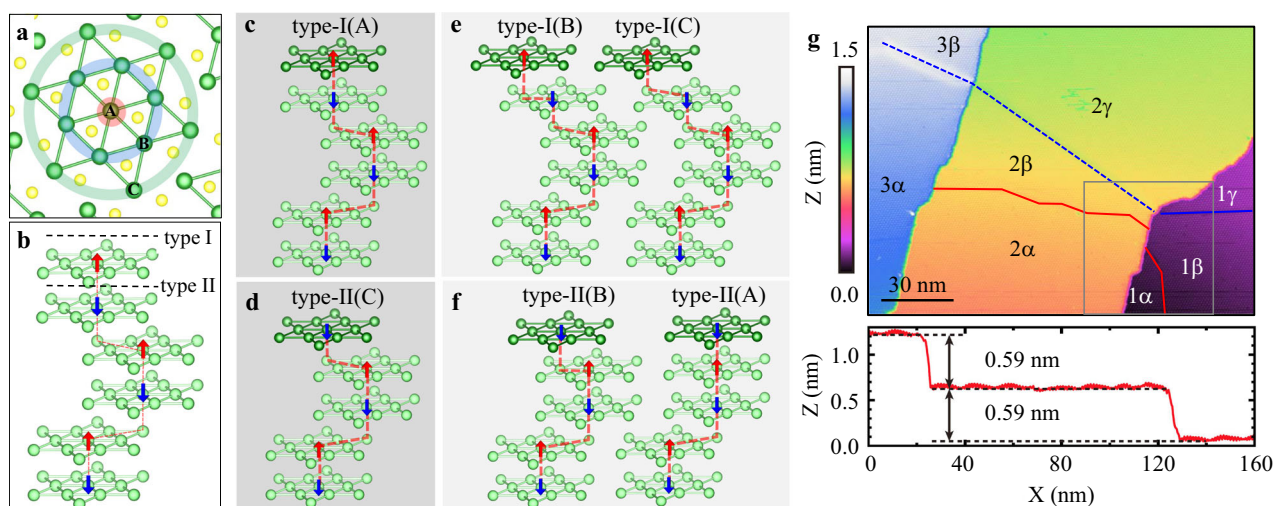

Fig. 1 Atomic structure and stacking order of the 1T-TaS$_2$ surface. a Atomic structure of the commensurate CDW phase (top view). **b** AC stacking order in the bulk (side view). Arrows indicate the spin components of the layer-by-layer antiferromagnetic order. **c** Type-I termination. **d** Type-II termination. **e**, **f** Stacking fault structures for the type-I and type-II surfaces, respectively. **g** STM topographic image with three terraces (top panel) and STM height profile (bottom panel). Three terraces (1: blue, 2: yellow, and 3: purple) are separated by domain walls (solid and dashed lines) denoted by α, β, and γ. The solid line and the dashed line represent the domain walls of the top layer and the sublayer, respectively.
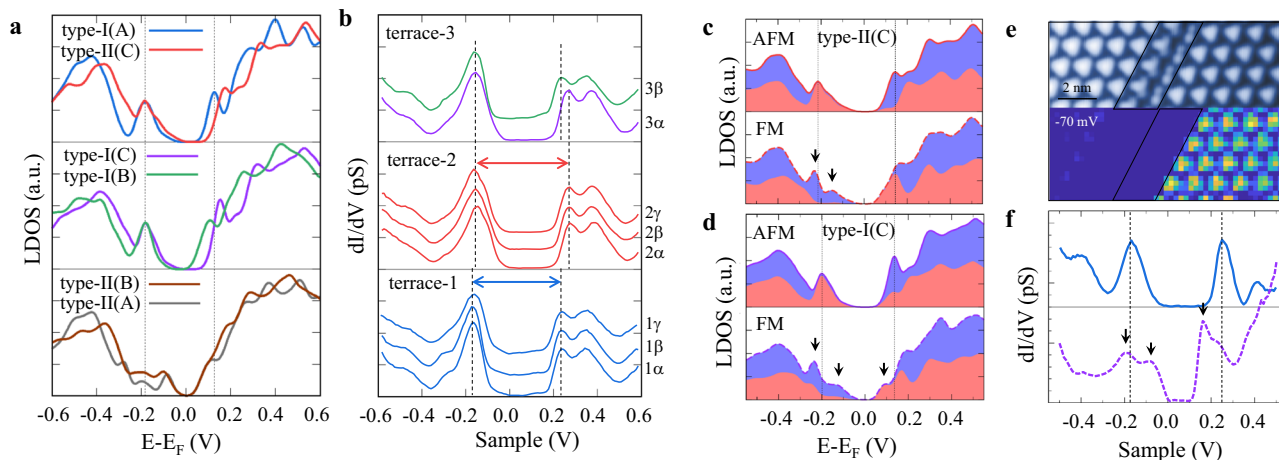
Fig. 2 Stacking-dependent electronic structure of the 1T-TaS₂ surface. a Theoretical LDOS of antiferromagnetic ordered surface. Dashed lines denote the band gap of the type-I(A) stacking for guide eyes. For better comparison, we shifted the Fermi levels by −0.03 to 0.03 eV to set the LHB states at the same position. **b** STS spectra at each domain of Fig. 1g. Dashed lines and arrows denote the size of the band gap for guide eyes. **c** Theoretical LDOS of the antiferromagnetic and ferromagnetic ordered type-II(C) stacking structure. Red and blue areas denote the major and minority spin components, respectively. **d** is for type-I(C) stacking structure. **e** STM topographic image and dI/dV map of two domains separated by a domain wall. Solid lines represent a double row of domain walls. **f** STS spectra for the right (top panel) and left (bottom panel) domains in (**e**).

limit[12,15] and the FM coupling between the top and the second layer would be an excited state. We calculate twelve slab models in total including six shown in Fig. 1 and their FM excited states. The energetics, including the vdW energy, the Coulomb energy of U, and their combination (vdW + U), for all considered stackings, are summarized in Supplementary Note 1 and Table I. In addition, the layer-resolved local magnetic moments for the DFT+U calculations are summarized in Supplementary Table II. Most of the bilayer-coupled stacking orders converge to an AFM order, but an unpaired single-layer can exhibit an FM coupling, which can also affect the electronic structure. We will discuss this in more detail below.

Antiferromagnetic surface layers. We first explain the electronic structures of six different stackings with an interlayer AFM order[12,15]. The top panel of Fig. 2a shows the local density of states (LDOS) calculated for type-I and -II terminations (see also Supplementary Note 2 and Supplementary Figs. 1–3). The type-I termination with A stacked bilayer exhibits a large gap of 0.31 eV and the band gap in the type-II termination with C stacking is similar but increases by 0.05 eV. This result contradicts the previous interpretation of the STS study of large (0.4 eV) and small (0.2 eV) gaps for the A and C stackings, respectively[10], but consistent with an identical band gap of both the A and the C stackings reported in a more recent STS study[14]. Note that the theoretical band gap at U = 2.3 eV is smaller than the experimental band gap most likely due to an underestimation of the correlation effect at the surface limit (Supplementary Note 3 and Supplementary Fig. 4). In our previous work with alkali metal adsorbates, the surface termination after the alkali adsorption could not be clearly determined and we considered only the isolated double- and single-layer models[13]. This indicates that the single-layer band gap does not explain the case of a surface-terminated layer. However, since a few STS experiments observed a small gap of about 0.2 eV consistently, there can be a surface layer with a largely different size of the band gap from the two above cases in DFT calculations.

As mentioned above, each type-I and -II termination has two other surface terminations through stacking faults. The stacking-fault surface layers, the B and C stackings, in the type-I termination, exhibit band gaps of 0.29 and 0.34 eV, respectively (the middle panel of Fig. 2a), which are slightly larger or smaller compared to the 0.31 eV of the type-I termination without a stacking fault. This is

consistent with the recent STS observation of almost identical band gaps of about 0.4 eV for A–C stackings between the top two layers[14]. In stark contrast, the band-gap sizes of the A and B stacking-fault surfaces of the type-II termination are dramatically reduced to 0.15 eV (the bottom panel of Fig. 2a). This difference is mainly due to the stacking order between the second and the third layer as discussed further below. Note also that, in the A stacking orders, the type-II(A) termination has not been observed in experiments, but only the type-I(A) termination with a large gap is observed. In conclusion, some of the surface layers with the intrabilayer termination (type-II) can have a much-reduced band gap, and the size of the band gap does not have a one-to-one correspondence with the stacking order between the top and the second layers. Since this is related to the existence of the stacking fault in the bulk AC stacking order, its appearance on the surface can depend largely on samples. We believe that this partly explains the different experimental observations in terms of the band gap and the terminations. In fact, our own experiments with a few different samples provide largely different chances to observe a surface layer with a small band gap. Moreover, we frequently observe slightly different band gap sizes (by about 0.05 eV) in neighboring terraces. Figure 1g shows an STM topographic image of the 1T-TaS₂ surface with three terraces, marked by 1–3, separated by two-step edges. Each terrace is further divided into several domains by domain walls as indicated by dashed lines. Three domains in the first terrace (1α, 1β, and 1γ) exhibit an identical large gap of about 0.4 eV (bottom panel in Fig. 2b). Meanwhile the domains in the second terrace (2α, 2β, and 2γ) also exhibit the large-gap states but with a slightly larger gap size compared to the first-terrace domains (see dashed lines in Fig. 2b). This observation is in good agreement with the present calculations for the type-I(A) and type-II(C) terminations of the bulk (see also Supplementary Note 4). One exception on the third terrace, two domains have distinguishable large gaps which are likely due to the presence of stacking faults on the type-II(c) of the second terrace. Considering the DFT results (middle in Fig. 2a), the larger-gap state in the 3α domain has to be the C stacking which corresponds to the type-I(C) surface.

Ferromagnetic surface layers. Since the interlayer AFM order of the bulk phase is basically due to the bilayer stacking order, the magnetic order of the unpaired top layer created by intrabilayer

termination can be uncertain. We examine the FM coupling between the top and second layers as excited states for all six stacking structures we considered. We find that the FM order is allowed only for the C stacking cases between the two topmost layers. In other cases, the initial FM order in the topmost layers is unstable and converges into the AFM order by spin flipping, or suppressing, for the case of the type-II(B), second-layer spins to result in the FM coupling between the second and third layers (see Supplementary Table II). On the other hand, the FM top layers in the C stacking exhibit almost degenerate energies with the AFM order (+1.1 and +0.36 meV/DS for the type-I and -II terminations, respectively).

The theoretical LDOS of the FM couplings in Fig. 2c and d shows a well-separated double peak structure at the top valence band. One peak is shifted to a higher energy compared to the single peak [the lower Hubbard band (LHB)] of the AFM coupling cases and the other to a lower energy to result in a reduced band gap size. These two peaks are in good agreement with the characteristic valence band structure of the small-gap cases reported for the C stacking in the present STS spectra of Fig. 2e and f and in the previous STS studies (see also Supplementary Note 4)[10,13]. That is, some C stacked layers can have a small gap through a different interlayer spin coupling, which explains the experimental observations of a small gap in some C stacking cases. The modulation of the band gap in the C stackings, induced by the local spins within the single-layer-like structure, does not contradict with the absence of magnetic ordering in the AC(bilayer)-stacked bulk. The magnetic properties of this material continue to be a subject of debate even within the bulk, and there have been no studies conducted on surface layers[12,17]. In conclusion, the above calculations indicate clearly that there exist two extra control parameters for the band gap of the surface layer, which have not been considered so far, such as the layer stacking between the second and the third layer and the spin ordering between the first and the second layer.

Experimental stacking orders. We have further investigated the stacking order through direct observations of STM images at the steps as shown in Fig. 3. The experimental analysis in Fig. 3a and b reveals that both the 2α and 2γ domains exhibit the A stacking order, which appears to be in conflict with the theoretical expectations. However, upon considering the phase shift induced by domain walls, it becomes apparent that the 2β domain exhibits a distinct stacking order (C stacking) from the 2α and 2γ domains (see Supplementary Fig. 5). The spectrum of the 2β domain is

identical to those of 2α and 2γ domains (Fig. 2b). This also conflicts with the stacking-dependent theoretical results.

As one way to address this discrepancy, we hypothesized the presence of a domain wall just below the step edge at the first layer (Fig. 3d). This is because it is difficult to identify whether a domain wall exists below the step edge in the STM image or not. Moreover, it should be noted that when cleaving the bulk sample, it may tear along energetically unstable areas such as domain walls (right panel in Fig. 3d and Supplementary Fig. 6). If we assume the existence of the most popular domain wall type DW-2, then all three domains in the second terrace exhibit a C stacking order (Supplementary Fig. 5c). This is consistent with both theoretical predictions and experimental observations. Furthermore, outside of the present data set, it has been frequently reported that identical STS spectra are observed for two domains separated by a domain wall[18–22], indicating the existence of the same type of domain wall at the top and the second layers. It was also directly observed that a domain wall in the top layer can be easily accompanied by a domain wall in the second layer, which is confirmed by a theoretical model[23,24]. Additionally, we found a case where a domain wall in the second layer merges with a domain wall in the top layer, and a formation of domain wall along the step (see Supplementary Fig. 7). Note also that, even in the absence of assuming a sublayer domain wall, there is a significant possibility that the domain wall can form along the step (Supplementary Fig. 6). Therefore, the current assumption of a hidden domain wall appears routed in the experimental data themselves and proposes to resolve the inconsistency within the experiments and make the theoretical predictions fit with the experimental data.

Origin of surface band gaps. In order to understand the origin of the small and large band gaps, we look into the band structures calculated for different stacking and spin orders as shown in Fig. 4. Each slab exhibits five or six bands between −0.2 and 0 eV which originate from localized Ta d electrons at DS centers in each layer of the five and or six-layer slab. The A-stacked bilayer structure with the AFM ordering of the type-I(A) surface shows the hybridized states of the first and the second layers due to the direct interlayer bonding. The band gap is due mainly to the bonding–antibonding splitting (~0.24 eV), which is, however, enhanced by the Coulomb interaction (by 0.07 eV at $U = 2.3$ eV) (Supplementary Fig. 2 and Fig. 4). For the C stacked layer within the AFM order, for examples, the type-I(C) surface in Fig. 4b, the bands on the surface layer are naturally much less affected by the
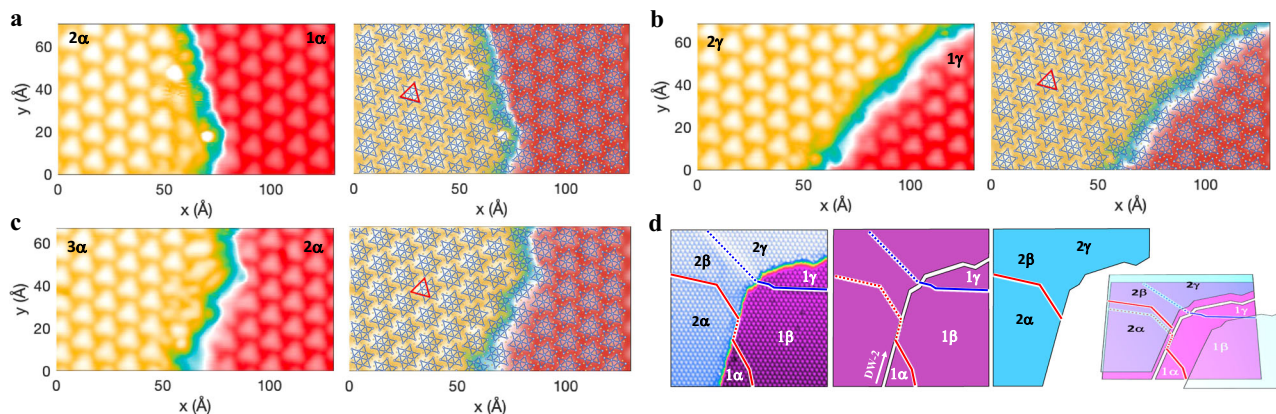

Fig. 3 Experimental stacking orders and a hidden domain wall. a–c STM images at step edges crossing domains (**a**) 2α–1α, (**b**) 2γ–1γ, and (**c**) 3α–2α. David stars represent the arrangement of protrusions in the lower terrace, while that of the top terrace is depicted as a triangle. **d** Wide-view STM image of the square-box region in Fig. 1g and schematic images for the domain wall configuration in the first (purple) and second (blue) terraces. White lines denote the hidden domain wall along the step edge. Right panel shows the region peeled off during the cleaving process.
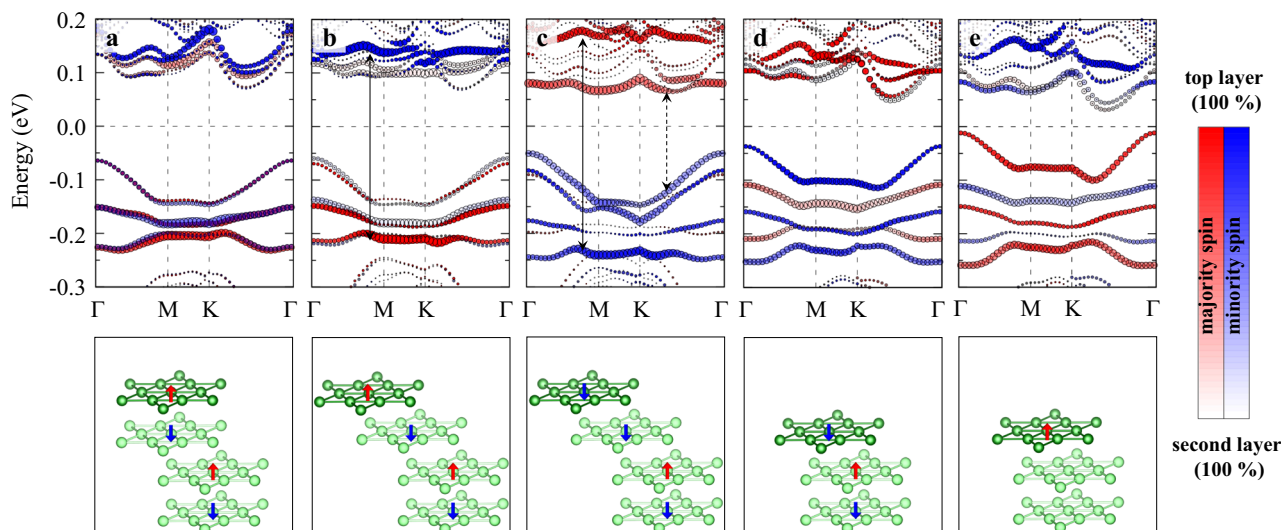
Fig. 4 Band structures of stacking and spin orders. a–e Band structure (top panels). The circle size is proportional to the state localized at the central Ta atom of the top- and second-layer DS cluster. Red and blue circles denote the majority spin and the minority spin, respectively. The color gradient indicates the strength of the localized state from the top to the second layer. Bottom panels correspond to their atomic structure with a schematic spin orientation. In **e**, the local magnetizations of the second and third layers are suppressed (see also Supplementary Table II).

interlayer coupling and maintain the Mott insulating state as in the 2D single layer [LHB and upper Hubbard band (UHB)] are marked by solid arrow in the Fig. 4b]. In the ferromagnetically coupled C stacking, the UHB (LHB) state is shifted downward (upward) compared to the AFM case and additional hybridized states appear between -0.15 and -0.05 eV and at around $+0.1$ eV (see dashed arrow in Fig. 4c). Thus, the small band gap itself is defined by the hybridized states of the surface and the second layers. Despite the reduction in the gap due to hybridization, the original Mott state persists (solid arrow in Fig. 4c), and without the on-site Coulomb energy, it becomes a half-filled state (Supplementary Fig. 2)[15]. Therefore the ferromagnetically coupled C stacking is a Mott insulator, which is distinct from the A stacking with a bonding-antibonding gap without a correlation effect (Supplementary Fig. 2).

In the type-II(B) stacking surface (Fig. 4d), the surface layer bands are located mainly at around -0.05 eV which is well within the band gap of the bulk. The change in the spin configuration (suppression of AFM order in this case) leads to an upward shift of the energy levels of the sublayers and reduces further the size of the band gap down to 0.05 eV (Fig. 3e and Supplementary Fig. 3). This seems to explain the partial-gap-like quasi-metallic spectra observed in the previous STS studies[10,14]. On the other hand, the type-I(B) surfaces exhibit large gaps. A major difference from the type-II surface is that the second layer exhibits a Mott insulating state, resulting in relatively weak interlayer coupling (Supplementary Fig. 2).

Discussion

The physics behind the effects of the stackings and spin orderings can be understood by a one-dimensional tight-binding atomic chain model along the C axis (Supplementary Note 5 and Supplementary Fig. 8[25]). In this model, the spin-singlet Z_2 dimerized chain having two distinct, trivial (corresponding to the A-stacked bilayer surface) and nontrivial (corresponding to the C-stacked surface), topological edge states. The additional application of on-site energy to the edge states not only manifests the dimer states localized at the edge (A-termination surface) but also explains well the tendency of the topological zero mode (C-termination surface) to diverge into the bulk states with single or double branches depending on the AFM and FM configurations, as

indicated by DFT results. This model calculation provides a picture of trivial and topological edge states of a spin singlet dimer chain under strong electron correlation in understanding the surface state of 1T-TaS$_2$. Furthermore, we propose that in order to achieve a comprehensive understanding of phenomena such as the spin liquid phase, a model that considers both magnetic order and interlayer coupling is necessary[26]. The present work indicates the importance of interlayer coupling in both charge and spin degrees of freedom in stacked Mott insulating layers and proposes to resolve the outstanding discrepancy between different experimental observations on the surface band gap of 1T-TaS$_2$.

Methods

Density-functional theory calculation. DFT calculations were conducted using the Vienna ab initio simulation package[27] and involved the application of the Perdew–Burke–Ernzerhof generalized gradient approximation[28] and the projector augmented wave method[29]. We used a plane-wave basis set of 400 eV, an $8 \times 8 \times 1$ k-point mesh for the $\sqrt{13} \times \sqrt{13}$ unit cell, and a force criterion of 0.01 eV/Å. The slab consists of six (type-I) and five (type-II) Ta layers with an equilibrium lattice constant of 3.374 Å and a vacuum spacing of about 13.6 Å. The interlayer distance is fixed at the experimental value of 5.9 Å. In order to represent electronic correlation, an on-site Coulomb energy of $U = 2.3$ eV was included for Ta 5d orbitals[15,30]. This value offers a more comprehensive explanation for the experimental gap in contrast to the recently proposed small U value of about 1.3 eV[31], and it aligns well with the band gap size found in more elaborated calculations using the GW approximation and the extended dynamical mean-field theory[32]. We utilized the Tkatchenko–Scheffler method for the van der Waals (vdW) calculations[33]. For the tight-binding model calculations, we used the PythTb package by Coh and Vanderbilt[34].

Scanning tunneling microscopy measurements. A single crystal of 1T-TaS$_2$ was cleaved in a high vacuum to obtain clean surfaces. STM measurements were performed at 4.4 K in constant-current mode with a sample bias of -0.6 eV. Scanning tunneling

spectroscopy was performed using a lock-in technique with a modulation frequency of 1 kHz.

Data availability

References

1. Sipos, B. et al. From Mott state to superconductivity in 1T-TaS$_2$. *Nat. Mater.* **7**, 960 (2008).
2. Stojchevska, L. et al. Ultrafast switching to a stable hidden quantum state in an electronic crystal. *Science* **344**, 177 (2014).
3. Park, J. W., Cho, G. Y., Lee, J. & Yeom, H. W. Emergent honeycomb network of topological excitations correlated charge density wave. *Nat. Commun.* **10**, 4038 (2019).
4. Lawa, K. T. & Lee, P. A. 1T-TaS$_2$ as a quantum spin liquid. *Proc. Natl Acad. Sci. USA* **114**, 6996 (2017).
5. Klanjšek, M. et al. A high-temperature quantum spin liquid with polaron spins. *Nat. Phys.* **13**, 1130 (2017).
6. Brouwer, R. & Jellinek, F. The low-temperature superstructures of 1T-TaSe$_2$ and 2H-TaSe$_2$. *Physica B+C* **99**, 51 (1980).
7. Fazekas, P. & Tosatti, E. Electrical structural and magnetic properties of pure and doped 1T-TaS$_2$. *Philos. Mag. B* **39**, 229 (1979).
8. Ritschel, T., Berger, H. & Geck, J. Stacking-driven gap formation in layered 1T-TaS$_2$. *Phys. Rev. B* **98**, 195134 (2018).
9. Lee, S.-H., Goh, J. S. & Cho, D. Origin of the insulating phase and first-order metal–insulator transition in 1T-TaS$_2$. *Phys. Rev. Lett.* **122**, 106404 (2019).
10. Butler, C. J., Yoshida, M., Hanaguri, T. & Iwasa, Y. Mottness versus unit-cell doubling as the driver of the insulating state in 1T-TaS$_2$. *Nat. Commun.* **11**, 2477 (2020).
11. Ishiguro, T. & Sato, H. Electron microscopy of phase transformations in 1T-TaS$_2$. *Phys. Rev. B* **44**, 2046 (1991).
12. Shin, D. et al. Identification of the Mott insulating charge density wave state in 1T-TaS$_2$. *Phys. Rev. Lett.* **126**, 196406 (2021).
13. Lee, J., Jin, K.-H. & Yeom, H. W. Distinguishing a Mott insulator from a trivial insulator with atomic adsorbates. *Phys. Rev. Lett.* **126**, 196405 (2021).
14. Wu, Z. et al. Effect of stacking order on the electronic state of 1T-TaS$_2$. *Phys. Rev. B* **105**, 035109 (2022).
15. Jung, J., Park, J. W., Kim, J. & Yeom, H. W. Surface enhanced electron correlation on the trivial quasi-two-dimensional bulk insulator 1T-TaS$_2$. *Phys. Rev. B* **106**, 155406 (2022).
16. Wang, G. et al. Atomic visualization of the 3D charge density wave stacking in 1T-TaS$_2$ by cryogenic transmission electron microscopy. *Nano Lett.* **23**, 4318 (2023).
17. Kratochvilova, M. et al. The low-temperature highly correlated quantum phase in the charge-density-wave 1T-TaS$_2$ compound. *npj Quantum Mater.* **2**, 42 (2017).
18. Cho, D. et al. Correlated electronic states at domain walls of a Mott-charge-density-wave insulator 1T-TaS$_2$. *Nat. Commun.* **8**, 392 (2017).
19. Ma, L. et al. A metallic mosaic phase and the origin of Mott-insulating state in 1T-TaS$_2$. *Nat. Commun.* **7**, 10956 (2016).
20. Bu, K. et al. Possible strain induced Mott gap collapse in 1T-TaS$_2$. *Commun. Phys.* **2**, 146 (2019).
21. Skolimowski, J., Gerasimenko, Y. & Žitko, R. Mottness collapse without metallization in the domain wall of the triangular-lattice Mott insulator 1T-TaS$_2$. *Phys. Rev. Lett.* **122**, 036802 (2019).
22. Aaishwarya, A. et al. Long-lifetime spin excitations near domain walls in 1T-TaS$_2$. *Proc. Natl Acad. Sci. USA* **119**, e2121740119 (2022).
23. Yao, Q., Park, J. W., Oh, E. & Yeom, H. W. Engineering domain wall electronic states in strongly correlated van der Waals material of 1T-TaS$_2$. *Nano Lett.* **21**, 9699 (2021).
24. Yao, Q., Park, J. W., Won, C., Cheong, S.-W. & Yeom, H. W. Kinkless electronic juction along one dimensional electronic channel. arxiv:2309.01648 [cond-mat.str-el] (2003).
25. Popescu, V. & Zunger, A. Extracting E versus **k** effective band structure from supercell calculations on alloys and impurities. *Phys. Rev. B* **85**, 085201 (2012).
26. Li, C.-K., Yao, X.-P., Liu, J. & Chen, G. Fractionalization on the surface: Is Type-II Terminated 1T-TaS$_2$ surface an anomalously realized spin liquid? *Phys. Rev. Lett.* **129**, 017202 (2022).
27. Kresse, G. & Furthmüller, J. Efficient iterative schemes for *abinitio* total-energy calculations using a plane-wave basis set. *Phys. Rev. B* **54**, 11169 (1996).
28. Perdew, J. P., Burke, K. & Ernzerhof, M. Generalized gradient approximation made simple. *Phys. Rev. Lett.* **77**, 3865 (1996).
29. Blöchl, P. E. Projector augmented-wave method. *Phys. Rev. B* **50**, 17953 (1994).
30. Darancet, P., Millis, A. J. & Marianetti, C. A. Three-dimensional metallic and two-dimensional insulating behavior in octahedral tantalum dichalcogenides. *Phys. Rev. B* **90**, 045134 (2014).
31. Lee, S.-H. & Cho, D. Charge density wave surface reconstruction in van der Waals layered materials. *Nat. Commun.* **14**, 5735 (2023).
32. Kim, T. J., Jeong, M. Y. & Han, M. J. First principles investigation of screened Coulomb interaction and electronic structure of low-temperature phase TaS$_2$. *iScience* **26**, 106681 (2023).
33. Tkatchenko, A. & scheffler, M. Accurate molecular Van der Waals interactions from ground-state electron density and free atom reference data. *Phys. Rev. Lett.* **102**, 073005 (2009).
34. Coh, S. & Vanderbilt, D. pythTB http://www.physics.rutgers.edu/pythtb (2016).

Acknowledgements

Author contributions

J.W.P. and H.W.Y. conceived the research idea and plan. J.W.P. performed the DFT calculations. J.L. carried out STM measurement. J.W.P. and H.W.Y. prepared the manuscript.

Competing interests

The authors declare no competing interests.

Additional information

Supplementary information The online version contains supplementary material available at https://doi.org/10.1038/s43246-023-00425-9.

Correspondence and requests for materials should be addressed to Jae Whan Park or Han Woong Yeom.

Peer review information *Communications Materials* thanks the anonymous reviewers for their contribution to the peer review of this work. Primary Handling Editor: Aldo Isidori. A peer review file is available.

Reprints and permission information is available at http://www.nature.com/reprints

Publisher's note Springer Nature remains neutral with regard to jurisdictional claims in published maps and institutional affiliations.